

EROSION-CORROSION PERFORMANCE OF HVOF SPRAYED WC-10CO COATINGS USING RESPONSE SURFACE METHODOLOGY

¹ Daniel C. Ribu, ²R.Rajesh, ³ D. Thirumalaikumarasamy*, ⁴ R. Paventhan
and ⁵ M. Ashok kumar

¹Daniel C. Ribu

Assistant Professor,

Department of Mechanical Engineering, Lourdes Matha College of Science and Technology,
Thiruvananthapuram – 608 002, Kerala, INDIA.

Email: ribucdaniel@gmail.com Tel: +91-09995453358 (Mobile)

²R.Rajesh

Professor and Principal

Department of Mechanical Engineering, Rohini College of Engineering & Technology,
Anjugramam– 629401, Tamil Nadu, INDIA.

Email: rajesh1576@yahoo.co.in Tel: +91-09894434131 Fax: +91-4652-266605

³D.Thirumalaikumarasamy (Corresponding Author)*

Assistant Professor,

Department of Mechanical Engineering, Government College of Engineering,
Bargur– 635104, Krishnagiri. Tamil Nadu, INDIA.

Email: tkumarasamy412@gmail.com, Tel: +91-09894319865(Mobile) Fax: +91-4144-
238080/238275

⁴ R.Paventhan

Professor

Department of Mechanical Engineering, Er.Perumal Manimekalai College of Engineering,
Krishnagiri- 635117. Tamil Nadu, INDIA.

Email: mr_paventhan@yahoo.com, Tel: +91-09944013323(Mobile) Email:
sreesabaridec2006@gmail.com

⁵M.Ashok kumar

Doctoral Research Scholar

Department of Mechanical Engineering, Government College of Engineering,
Bargur– 635104,

Krishnagiri. Tamil Nadu, INDIA.

Email: ashokleadsaero12@gmail.com

Abstract

In this study, conventional WC-12Co composite coatings were deposited on the steel substrate by HVOF, respectively. Structures of the coatings were analysed with SEM and XRD methods, and microhardness, porosity and roughness were also measured. Furthermore, the erosion corrosion experiments were carried out on the coatings to explore the effect of rotational speed and angle of impingement on the erosion corrosion behaviours. Electrochemical corrosion performance of the coatings and substrate were studied using potentiodynamic polarization test in sodium chloride environment. An attempt was also made to develop an empirical relationship to predict the erosion rate of coatings. Three factors five level central composite rotatable design matrix was used to minimize the number of experimental conditions. Response surface methodology was used to develop the relationship. The developed relationship can be effectively used to predict the erosion rate of coatings at 95% confidence level. Results reveal that the WC-12Co coatings provided the superior erosion corrosion performance than the uncoated substrate.

Keywords: Erosion-corrosion; WC-12Co; HVOF; RSM

Abbreviations:

HVOF: High velocity oxy fuel

HVAF: High velocity air fuel

SE: Slurry erosion

RSM: Response surface methodology

SEM: Scanning electron microscopy

XRD: X-ray diffraction

LPG: Liquefied petroleum gas

1. Introduction

Slurry erosion is a mechanical phenomenon. Equipment handling the slurry suffers damage through the impact of liquid borne solid particles, causing plastic deformation and / or material removal. In practical cases, slurries are often corrosive and the surfaces are degraded not only due to erosion but also owing to electrochemical corrosion. Both erosion and corrosion processes may act synergistically to cause more damage than the simple sum of the damage caused through each process individually. The blades of large centrifugal air compressor impellers operating under marine environment are generally subject to corrosion from the salty coastal air and erosion of solid particles, commonly resulting in corrosion rust and erosion wear [1, 2]. Therefore, the improvement of the corrosion and the erosion resistance of the impeller blades by using surface treatment technology are crucial. To date, scholars have found that the thermal spraying technology is an effective method for enhancing surface functionality [3] due to its advantages, such as minor thermal stress and small heat-affected zone. Therefore, the interaction mechanism between erosion and corrosion of coatings is an important research topic.

Thermally sprayed coatings have been widely used in the fields of aerospace, petrochemical

engineering, and marine engineering equipment due to its resistance against corrosion [4], wear [5, 6], and erosion [7]. The mechanical properties [8], deposition behavior [9], and wear behavior [10] of coatings have been widely investigated under varying circumstances (damage mode, particle size, and temperature). Porosity is clearly a dominant factor affecting the erosion and corrosion performance [11].

HVOF and HVAF have been considered to be the industrial standard for spraying carbide composite coatings [10, 11] and characterized by their low decarburization and excellent bonding [12].

Investigations have shown that WC-10Co is a promising alternative to hard chromium, but its corrosion performance is remarkably affected by the service circumstance [9-12]. Some attempts have been made to explore the influence of the combined action on the failure behavior. However, the combined action in WC-10Co coatings is still unclear especially in the erosion behavior under ultrafine particles (about 30 μm). The wear loss in seawater or rainwater is larger than that in distilled water in the fretting wear behavior of the micro-arc oxidation Al_2O_3 coating, which is attributed to the effect of the Cl^- ion and its accelerating influence on the wear process.

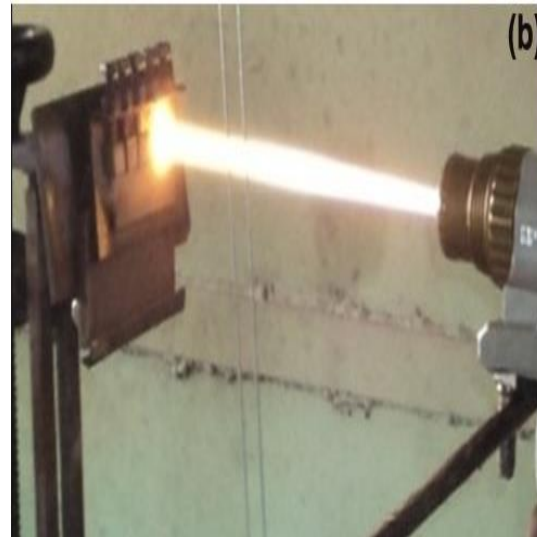
2. Experimental

In this study, conventional powders were used for depositing WC-10Co coatings with the thickness of about 200 μm on a 35CrMo steel substrate by HVOF (HIPOJET-2700, Make: Metallizing Equipment Co. Jodhpur, India) system available at Annamalai University, India. The thickness of the coatings was measured by digital micrometer (with an accuracy of 0.001mm) after each and every run conditions. Coating thickness was achieved by varying the number of deposition passes. Photograph of HVOF spray machine and the coated specimens were shown in Fig.1. The substrate needs to be preheated before spraying: this was accomplished through one complete torch cycle at a pass velocity of 0.8 m/s, achieving a temperature of 120–180°C. The substrate samples with the size of 15 mm \times 10 mm \times 8 mm, whose sides had a chamfer with a length of 1 mm and an angle of 45°, were cleaned in acetone by ultrasonic cleaning instrument. Corundum, grit size of 320 \pm 500 μm was used to increase the surface roughness of the substrate. A surface roughness tester (Make: Mitutoyo, Japan; Model: Surf test 301) was used to measure the roughness and the average roughness of the substrate after grit blasting was found to be 5–10 μm . The composition of conventional powders, which were produced by Metallizing Equipment Co, is as follows: WC-90 wt-% and Co-10 wt-%. The size range of the particles in the powder is 15–45 μm . The process parameters of HVOF sprayed WC-10Co coatings are listed in Table 1.

2.1 Coating characterisation



HVOF spraying facility



Coating deposition

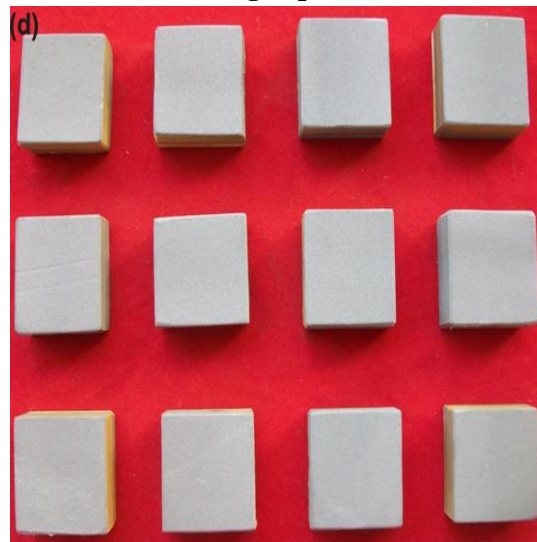
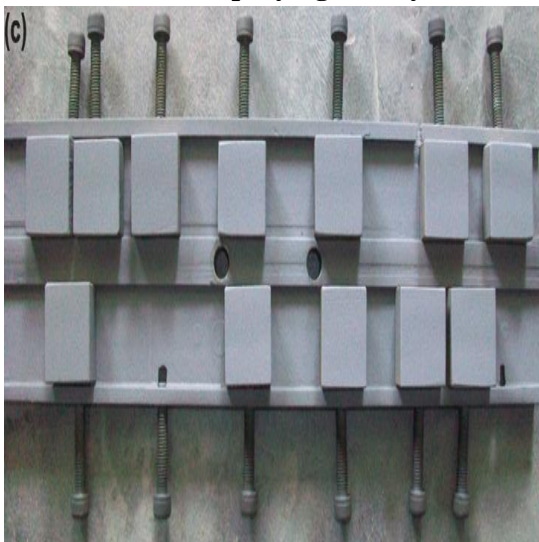


Fig.(c & d) Photographs of WC-10Co coated specimens

Fig.1 Experimental details.

Microstructural characterization of the powders and coatings was carried out by using scanning electron microscopy (Make: JEOL, Japan; Model: 6410-LV) to study the surface morphologies. Figure 2(a-b) shows the SEM image of the as-received powder with spherical morphology with a grain size range of $- 45$ to $+15 \mu\text{m}$. The narrow particle size distribution and spherical shaped particles improve higher melting efficiency and good flow ability. The cross sectional SEM images of coatings are shown in Fig. 2(c-d),

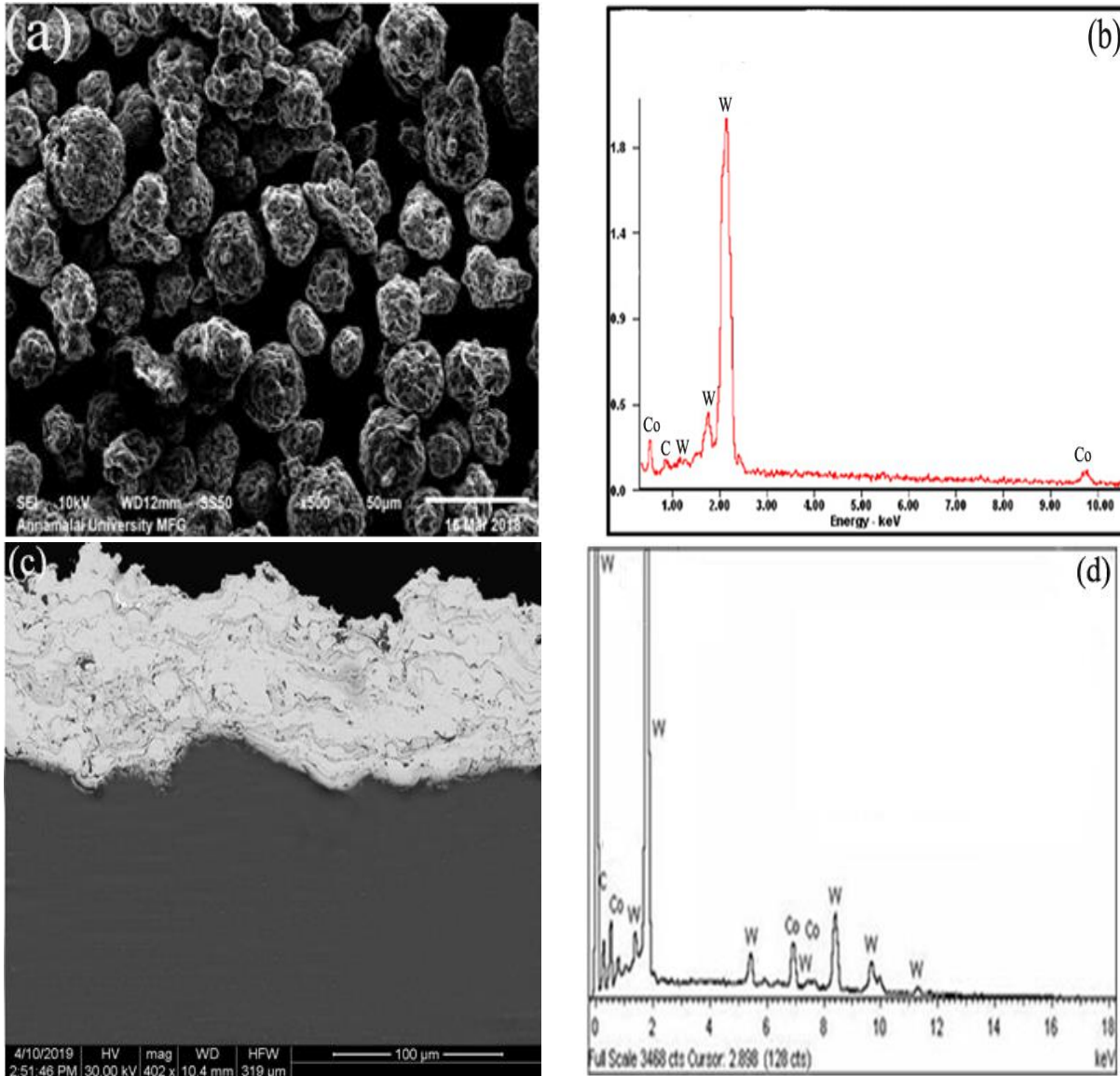


Fig.2 SEM images of WC-10Co powders (a&b) and sprayed coating surfaces (c&d)

respectively. It can be seen that the coating is very dense and has a good contact with the substrate. This indicates that the coating does have a tight adherence to the substrate due to the higher velocity of HVOF thermal spraying. Figure 3 shows the XRD patterns for the WC-10Co feedstock powder and the coating deposited by the HVOF process. The results showed that WC was the major phase identified. In the WC-10Co coating and the starting powder, different phases of W_2C , and Co_3W_3C were detected. The results revealed that higher flame velocity and lower flame temperature of the HVOF process would effectively limit WC decomposition process.

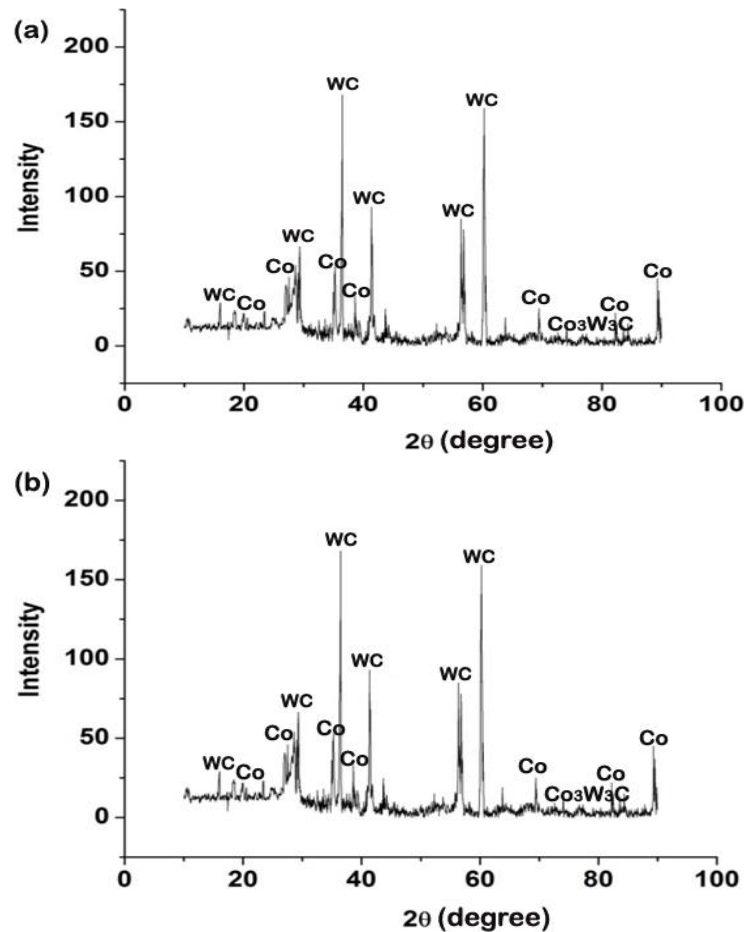


Fig. 3 XRD pattern of powder (a) and coating (b)

Table 1 HVOF process parameters

Process parameters	Values
Oxygen flow rate	253 lpm
LPG flowrate,	61 lpm,
Powder feed rate	35 g/min
Spray distance	227mm

Generally, porosity amount is very low in the coating produced by HVOF. This is because the high impact velocity of the coating particles causes high density and high cohesive strength of individual splats. According to the ASTM B 276 [13], the porosity measurement was carried out on the metallographically prepared cross sections of the coating, using optical microscope (Make: Meiji; Japan, Model: MIL-7100) equipped with an image analysing software (Metal vision version.6). In this investigation, the images captured under 1000x magnification by optical spectroscopy were chosen for porosity analysis to reveal the features of images like open pores and network of cracks standard. Initially, a 400 μm square area was selected on the polished cross-section of the coating and the image was analysed. The same procedure was repeated at

five random locations to find out the average percentage volume of porosity. The microhardness of coatings was measured using a microhardness tester (Make: Shimadzu; Japan. Model: HMV-2T) with a load of 2.94 N and hold time 15s. Hardness values were measured at 10 random locations on the polished cross-section of a coating. The fracture toughness of the coatings was measured using the HV-5 Vickers hardness tester according to the indentation cracking method performed on the cross section of coatings under a test

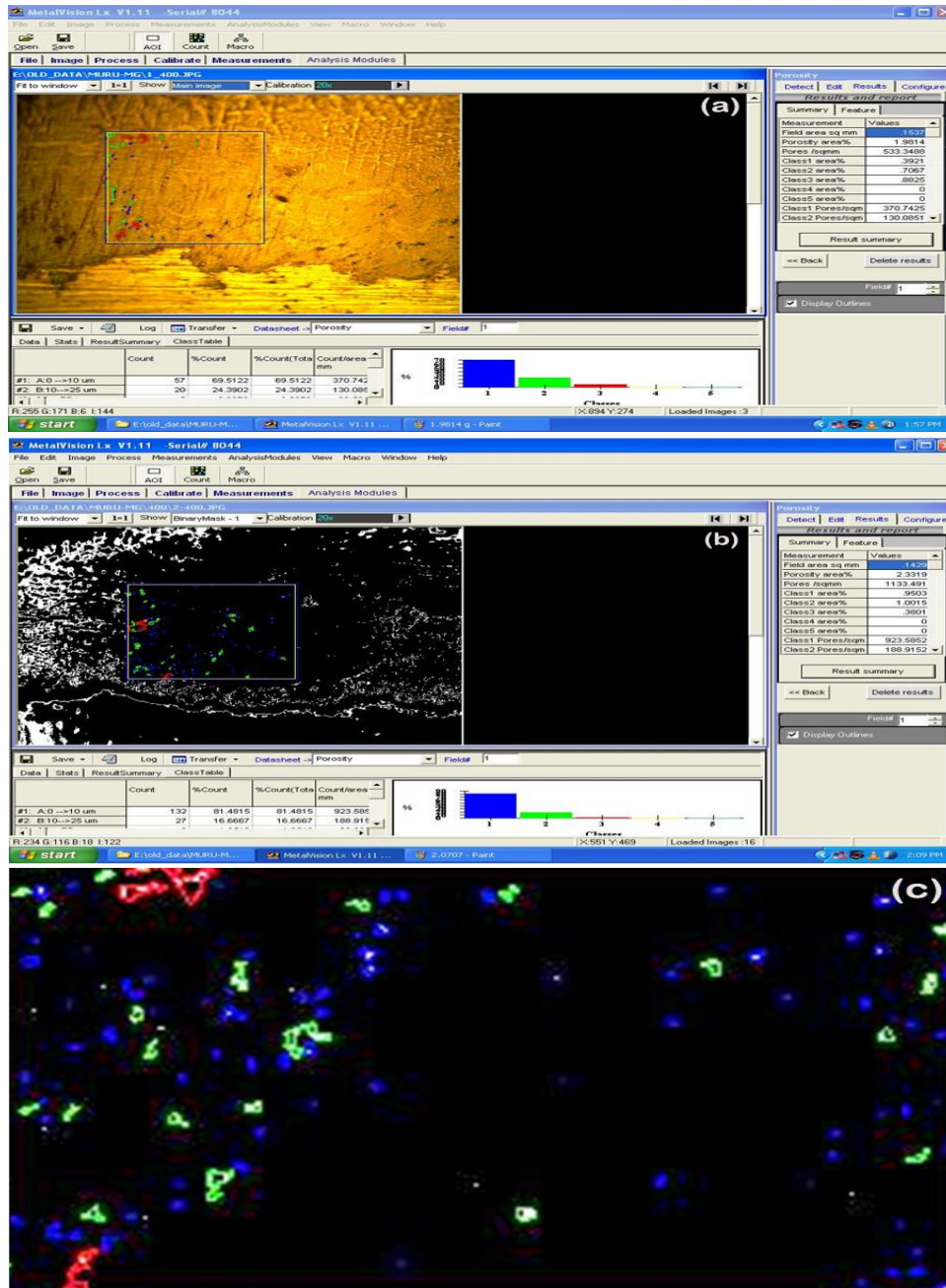


Fig. 4 Steps involved in image analysis; (a) Binary image of the selected image; (b) Selection of area to be analyzed (c) Color coded image after porosity analysis.

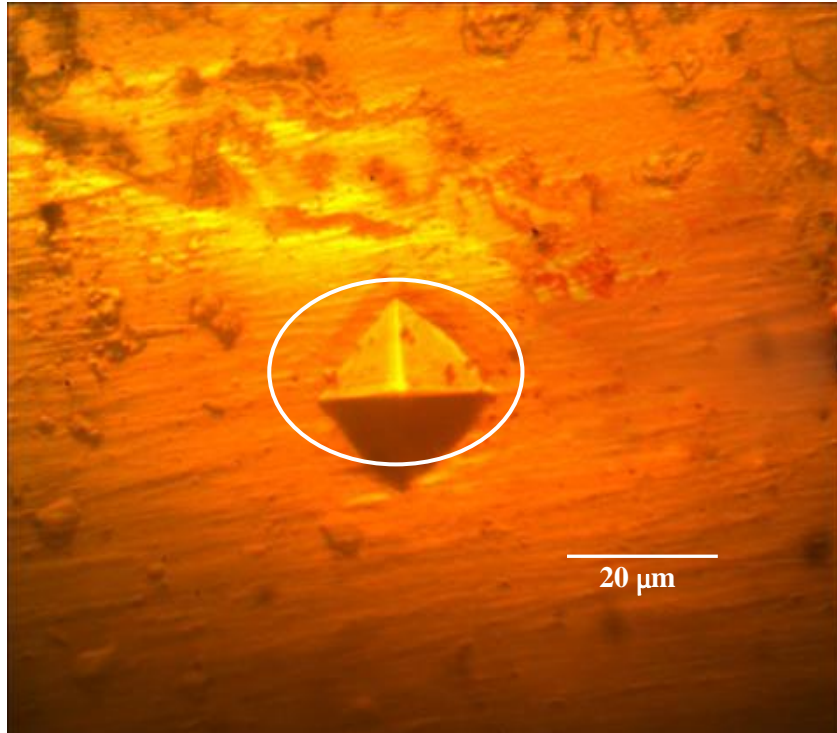


Fig. 5 Indentation image of coating produced under optimum condition

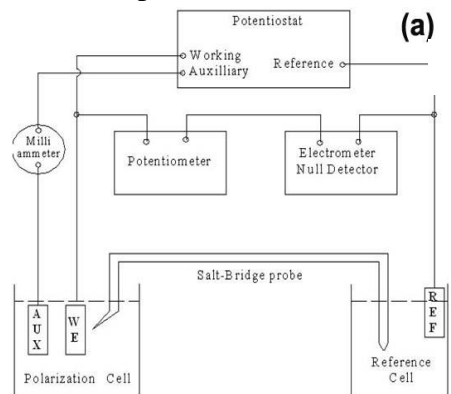
load 49 N and hold time 15 s. And the average values of 20 measurements were taken as the effective fracture toughness values. The images obtained through image analysis and hardness measurements were displayed in Figures 3&4. The bonding strength of the coating was tested according to the ASTM C-633-01 [14] requirement. The coatings sample was bonded with 35CrMo steel by using the E7 glue. After solidification, the measurement was carried out on a universal tensile test equipment (Make: FIE Blue Star; India. Model: UNITEK-94100). The crosshead speed of the equipment was 1 mm min⁻¹. The bonding strength of each coating is the average of three experimental measurements. The porosity level, micro hardness and bond strength of the as coated samples were 4 vol%, 1045HV and 8.99 MPa.

Synergistic erosion-corrosion test were carried out on ϕ 11 mm diameter specimens. Exposed area of the specimen is polished and ground to a smooth surface finish and the unexposed area is sealed/masked using lacquer. Specimens were weighed before and after test to determine the weight loss. A pot type slurry erosion-corrosion tester (Make: Wear and Friction Tech., Chennai; Model: WFT - SEC) was used for this investigation as shown in the Fig.6

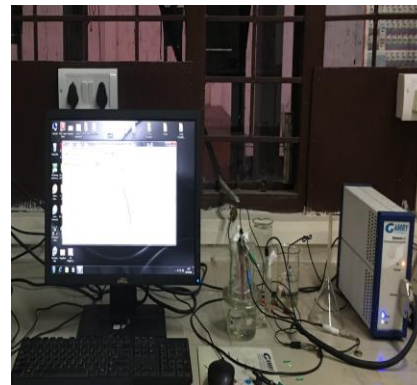


Fig. 6 Pot type slurry erosion-corrosion tester

The corrosion resistance of the coatings and 35CrMo steel was studied by electrochemical test with the aid of a Potentiostat / Galvanostat Model V5 (Gill AC, England) electrochemical system (Fig. 7). It was used to perform the cyclic potentiodynamic polarization test. Before test, samples were ground up to 1200 SiC papers and then degreased with acetone, washed with distilled water and dried in air following the guidelines of the standard ASTM G1-03. All electrochemical measurements were performed by using a standard three electrode system in 3.5 wt. % NaCl aqueous solution. The specimen is used



Schematic diagram of test set up



Photograph of test set up

Fig. 7 Details of potentiodynamic polarization test

as working electrode and the counter electrode was a silver rod and all potentials were monitored relative to a saturated calomel electrode (SCE) that connected to the cell. The exposure area of about 1 cm² of the coating in 3.5 wt. % NaCl aqueous solution was made open to air at room temperature. Experiments were started after immersing the specimens into the solution for 1 hour, when open circuit potentials became stable. Potentiodynamic polarization was swept from -500 to +1500 mV relative to the open circuit potential at a fixed rate of 0.5 mV /s .The cyclic polarization curve was measured with the potential sweep rate of 0.5 mV/s. The reverse potential

of the cyclic polarization experiments was 1.1 V. All measurements were repeated at least thrice to achieve precise results.

The E–C experiments set up consists of single spindle with specimen holder and a counter weight. The spindle is connected to a belt drive with a stepper motor. Spindle speed can be varied with the help of stepper motor and can be controlled using a Variable Frequency Drive (VFD). Based on the real time marine environment, the experiments were designed focusing on the effects of rotational speed, % of sand contained in slurry and exposure time on E–C performance. The silica sand with the particle size of 250 μ m has Average Fine Sieve number (AFS) 50 – 70.

After E–C test, the WC-10Co coatings and 35CrMo steel samples were washed with acetone, degreased, dried and weighted by using a digital balance with an accuracy of 0.1 mg. Scanning electron microscopy examinations were performed on surfaces of coatings and 35CrMo steel after E–C for different conditions to understand the progression of damage.

2.3 Formulating Experimental Design Matrix

After considering all of the feasible limits of the slurry erosion test apparatus as mentioned under the slurry erosion parameters and their limits were chosen, so that equipped with potentiodynamic polarization test apparatus wear test could be conducted without any difficulty. In order to study the effects of the slurry erosion parameters on the erosion rate, statistically designed experiments were used to reduce the time and cost. Tables 3 and 4 show the considered factors with their levels and erosion-corrosion rate for the uncoated and coated 35CrMo steel. In this investigation, the experiments were conducted in a random order to prevent systematic errors infiltrating the system. At least three experiments were carried out at each experimental condition to ensure reliability of the results. The erosion-corrosion experiments conducted in a corrosive slurry environment. The erosion-corrosion test specimens before and after experiments shown in Figure 8.

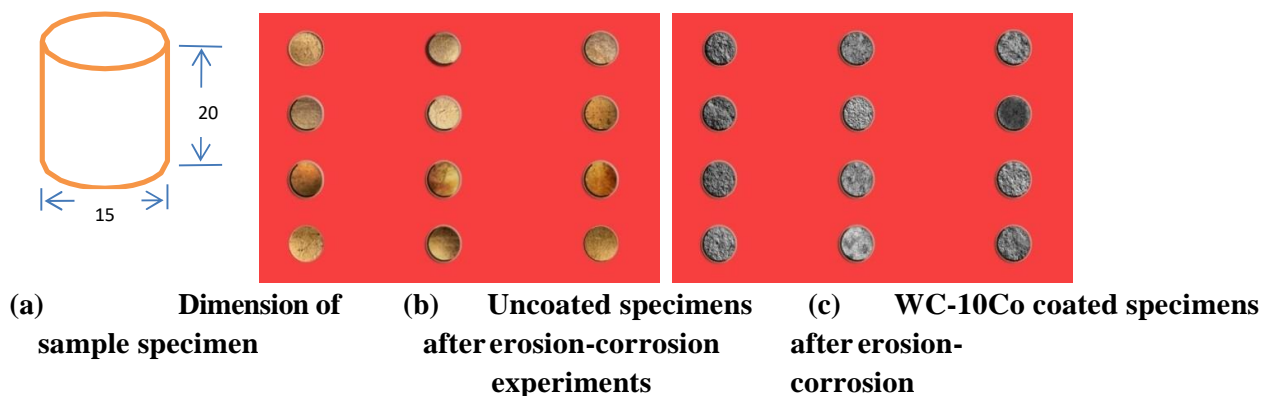


Fig. 8 Uncoated and coated specimens for erosion-corrosion experiments

3. Results and Discussion

Table 2 shows the mass loss of the uncoated and coated 35CrMo steel subjected to erosion-corrosion test conducted with various rotational speed, angle of impingement for the time period the table, that it is inferred that at low angle and low velocity mass loss is minimum whereas at high velocity and angle increased mass loss was observed.

3.1 Effect of angle of impingement on erosion-corrosion behavior

Figure 9 shows the SEM image of the uncoated 35CrMo steel exposed to various impingement angles. At lower impingement angles, the higher tangential and lower normal stress components induced by the slurry on the surface of specimens would introduce a longer sliding and cutting, therefore, a longer erosive track was observed. Successive impacts would further deform the lips and finally deformed lips can be detached from the surface as seen in Fig. 9.

However, due to the low normal stress and low penetration of the impacted slurry at an impingement angle of 30° , many impacts would be needed to remove the material from the surface, at resulted in a low erosion–corrosion rate. It is well known that at normal angle of impingement surface is not experience material removal in erosion. At lower impingement angle, one can see the increased mechanical erosion on the WC-10Co coated 35CrMo steel matrix and creating networks between the tungsten carbides within the coatings. Higher hardness and brittleness of the carbides suffer little erosion damage at lower angles. Low impingement angles creating longer wear scars, the longer the contact, the material is scratched and the electrochemical activity or corrosion increases. Coalescing of split particles resulting in a homogeneous 'ductile like' material that avoids preferential concentrated stresses at splat boundaries, which causes cracking and crack propagation forming macro pits that can be seen in Fig.9&10

Table 2 Total mass losses in free erosion-corrosion of uncoated and WC-10Co coated 35CrMo steel

Exp. No	Angle (deg)	Rotational speed (rpm)	Erosion (E)		Corrosion (EC)		Total mass loss TWL				Difference in mass loss	
			Mass loss (g)		Mass loss (g)		Mass loss (g)		Mass loss (g)		Mass loss (g)	
			Uncoated	coated	Uncoated	Coated	Uncoated	coated	Uncoated	coated	Uncoated	coated
1	45	750	0.41	0.15	0.00082	0.0000031	0.411	0.15	0.21	0.080	0.20	0.07
2	75	750	0.51	0.19	0.00102	0.0000038	0.511	0.19	0.27	0.099	0.25	0.09
3	45	1250	0.52	0.20	0.00104	0.0000039	0.521	0.20	0.27	0.101	0.25	0.09
4	75	1250	0.63	0.24	0.00126	0.0000047	0.631	0.24	0.33	0.123	0.30	0.11
5	30	1000	0.44	0.17	0.00088	0.0000033	0.441	0.17	0.23	0.086	0.21	0.08
6	90	1000	0.48	0.18	0.00096	0.0000036	0.481	0.18	0.25	0.094	0.23	0.09
7	60	500	0.39	0.15	0.00078	0.0000029	0.391	0.15	0.20	0.076	0.19	0.07
8	60	1500	0.49	0.18	0.00098	0.0000037	0.491	0.18	0.25	0.096	0.24	0.09
9	60	1000	0.46	0.17	0.00092	0.0000035	0.461	0.17	0.24	0.090	0.22	0.08
10	60	1000	0.47	0.17	0.00092	0.0000035	0.471	0.17	0.24	0.090	0.23	0.08
11	60	1000	0.46	0.18	0.00092	0.0000035	0.461	0.18	0.24	0.090	0.22	0.09
12	60	1000	0.45	0.18	0.00092	0.0000035	0.451	0.18	0.24	0.090	0.21	0.09
13	60	1000	0.46	0.17	0.00092	0.0000035	0.461	0.17	0.24	0.090	0.22	0.08

Researchers showed that synergistic effect of erosion–corrosion and pure erosion are same at an impingement angle 30° and 90° . Synergism at impingement angles of normal incident of slurry could cause some penetration or indentation on the surface with raised lips around the impact zone. The highest impact energy could be transferred from slurry to the surface at a normal angle and induce a thicker work hardened layer on the surface.

On single-phase materials, an eroding particle is free to scratch the surface on the other hand a particle is scratching the soft binding material, the hard phase will deflect its trajectory reducing the amount of material removed. Normally brittle material experiences higher erosion at higher impact angles. Higher volume fraction of the strengthening carbides hard phase particles (higher hardness) that resists the severe mechanical impact of the slurry particles.

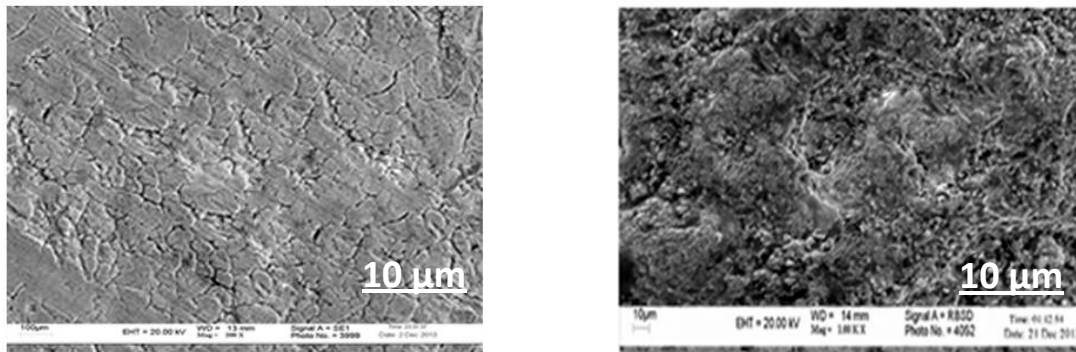


Fig. 9 SEM image of the erosion-corrosion tested uncoated and coated 35CrMo steel at slurry composition 600 g/cc, 30° , angle of impingement and rotational speed- 1000 rpm.

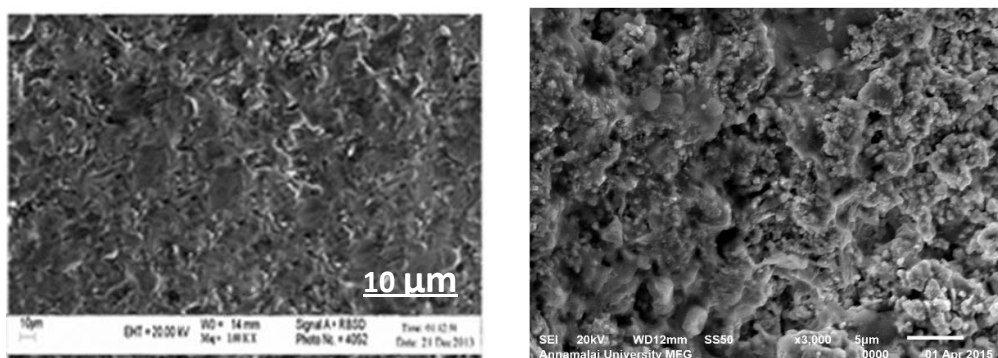


Fig. 10 SEM image of the erosion-corrosion tested uncoated and coated 35CrMo steel at slurry composition 600 g/cc, 90° , angle of impingement and rotational speed- 1000 rpm.

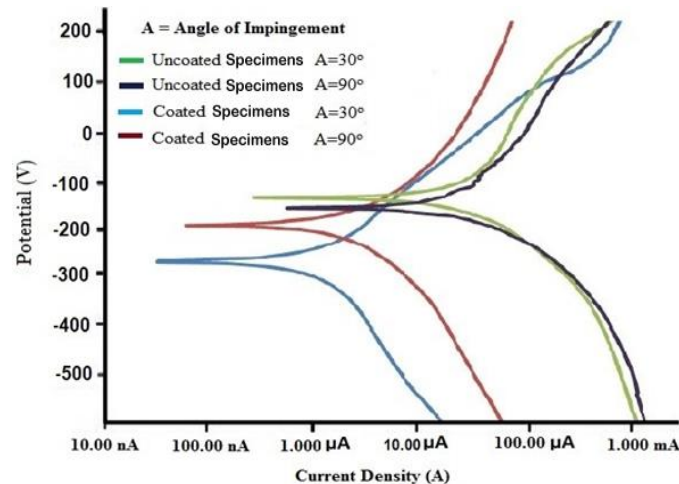


Fig. 11 Polarization curves for the uncoated and coated 35CrMo steel at various angle of impingement in 3.5 % NaCl solution

Total mass loss 'M' measurements showed (Table 2) a superior erosion-corrosion resistance of the coating compared with the 35CrMo steel having intermediate resistance the 35CrMo steel displayed 'ductile ploughing' effect. The mechanisms for the degradation of a WC-10Cocoating under a slurry impingement are as follows: in less severe erosion-corrosion condition (600 mg/l solids) corrosive effects could remove hard phase particles leaving a long thin spikes extending into the coating. These spikes or micro pits cause increased local turbulence which promotes the repeated impacts from solid particles in that area. The repeated impacts remove larger 'chunks' of the coating. Selective removal of the matrix is clearly more evident and indicating the operation of an erosion-corrosion damage mechanism. Certainly, cobalt matrix carbides are known to be more prone to erosion-corrosion damages. Under erosion-corrosion environment, coated 35CrMo steel shows higher erosion-corrosion mass when compared with uncoated 35CrMo steel. Figure 11 shows higher current density for uncoated 35CrMo steel, at higher constant speed of 1500 rpm and angle of impingement as 60° through extrapolation of the curve ($E_{\text{corr}}-248 \text{ mV}$ and $I_{\text{corr}}-18.4 \mu\text{A}/\text{cm}^2$) shows the current density is maximum and erosion-corrosion rate could be maximum whereas coating comprises WC, W_2C also experiences higher erosion-corrosion rate since the carbides are prone to corrosion [15].

3.2 Effect of rotational speed on erosion rate

From the fundamentals, it is obvious that the erosion rates increase with increase in rotational speed. As the erosion wear occurs due to the movement/kinetic energy of impacting particles, so it is quite expected that erosion rate will increase with the increase in the velocity of impacting particles. Increase the rotational speed, increase impact velocity and decreases the corrosion resistance of the 35CrMo steel. This could possibly be due to the effects of plastic deformation (Fig. 12) on the surface, at higher velocities leading to an increase in the exposure area for exposure to the corrosive environment.

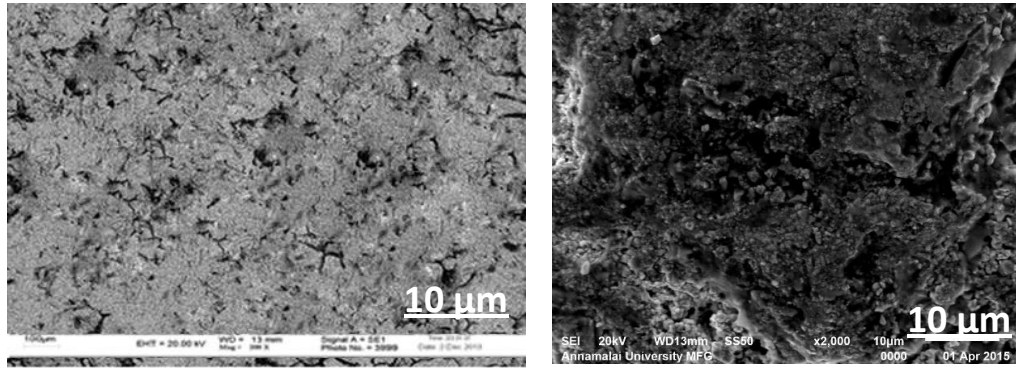


Fig. 12 SEM image of the erosion-corrosion tested uncoated and coated 35CrMo steel slurry composition 600 g/cc, angle of impingement at 60°, rotational speed 1000 rpm.

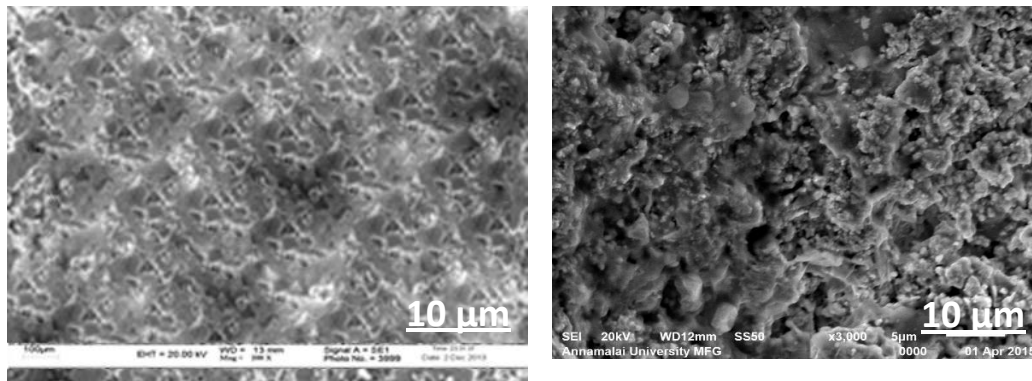


Fig. 13 SEM image of the erosion-corrosion tested uncoated and coated 35CrMo steel slurry composition 600 g/cc, angle of impingement at 60°, rotational speed 1000 rpm.

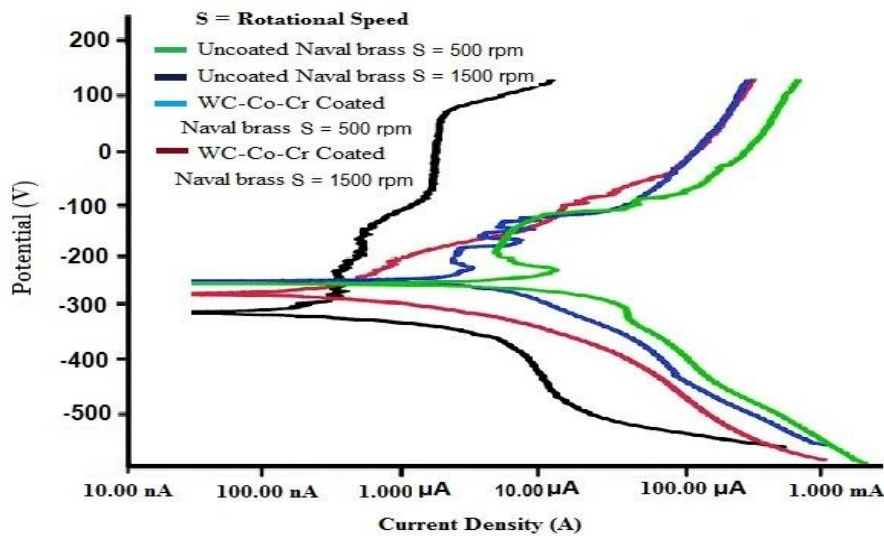


Fig. 14 Polarization curves for the uncoated and coated 35CrMo steel at various rotational speed 3.5 % NaCl solution

The general expression showing the dependency of erosion rate on be rebounding of more impacting particles from the target surface at higher impact velocity as compared to the same at lower impact velocity, which might have resulted in deviation of path of coming particles. Moreover as the particles were under constant movement due to steady flow, it is anticipated that whole of the kinetic energy of the particles might have not transferred to the target surface. Hence, the erosion- corrosion rate is minimum at low rotational speeds as shown figure 12.

It has been pointed that metastable pitting of 35CrMo steel in NaCl chloride solution is enhanced through exposure of correction environment during erosion, essentially increasing the surface area and this increase in surface area at the higher velocities and current density increases. WC-10Co coatings also exhibits a similar pattern of increasing corrosion current density to above -120 mV, with an increase in impact velocity as inferred from Fig. 14. In this case, the effect of velocity on the corrosion current density are much greater, possibly due to the removal of carbide grains at the higher velocities, leading to an increase in surface area of the binder for exposure to the corrosion in shown in Fig. 13.

4. Erosion, Corrosion and Synergy

The contributions of the total mass loss (M) were defined as erosion, E, corrosion, C, and a synergistic component; S, the contributions from each component and each component as a percentage of the total weight loss. At lower speed (500 rpm) for pure erosion, the measured total weight loss was found to be 0.15 mg after five hour's impingement. From calculations using Tafel Extrapolation and the corrosion component is found to be approximately 0.0000029 and in erosion and corrosion environment the mass loss found to be 0.076 mg. The measured weight loss under pure corrosion component was found to be small negligible. Due to the small weight loss measured and the large amount of error (± 0.1 mg), the calculated contributions of E, C and S at this solid content will be unreliable. However, as the speed it increased to 1000 rpm, the corrosion component is still very dominant at 59% after five hours impingement, incurring a negative synergistic component. In contrast to the previous negligible contribution from pure erosion at 700 rpm and 1000 rpm the pure erosion component contributes to 50% - 55% of the overall weight loss. At 1500 rpm solids content, the corrosive component still has a fairly significant contribution to the total weight loss (30% after 5 hours impingement), as is the indirect corrosive component's (synergy) contribution (15% after 5 hours impingement).

While at both speed, (1000 and 1500 rpm) the pure mechanical damage is 50% or more, the pure corrosive component both as an absolute value and as a percentage is reduced at the higher solid (Table 2). The corrosive component is only 6% in after 5 hours impingement. Again the pure erosive component has the most dominant contribution. A general trend of decreasing corrosion component, after five hour impingement, with increasing solid content exists while the synergistic component decreases. This synergistic effect has been found to be in excess of 40% of the total weight loss, decreasing with decreasing solid content. There

is however, is a considerable amount of material loss and signifies that the interaction of the erosion and corrosion mechanisms are very important in the identifying the cause of material wear.

The proposed mechanisms for the degradation of a WC-10Co coating under liquid solid slurry shows higher severe erosion-corrosion condition (1500 rpm) remove hard phase particles leaving long thin spikes extending into the coating. These spikes or micro pits cause increased local turbulence which promotes the repeated impacts over in that area. The repeated impacts remove larger 'chunks' of the coating.

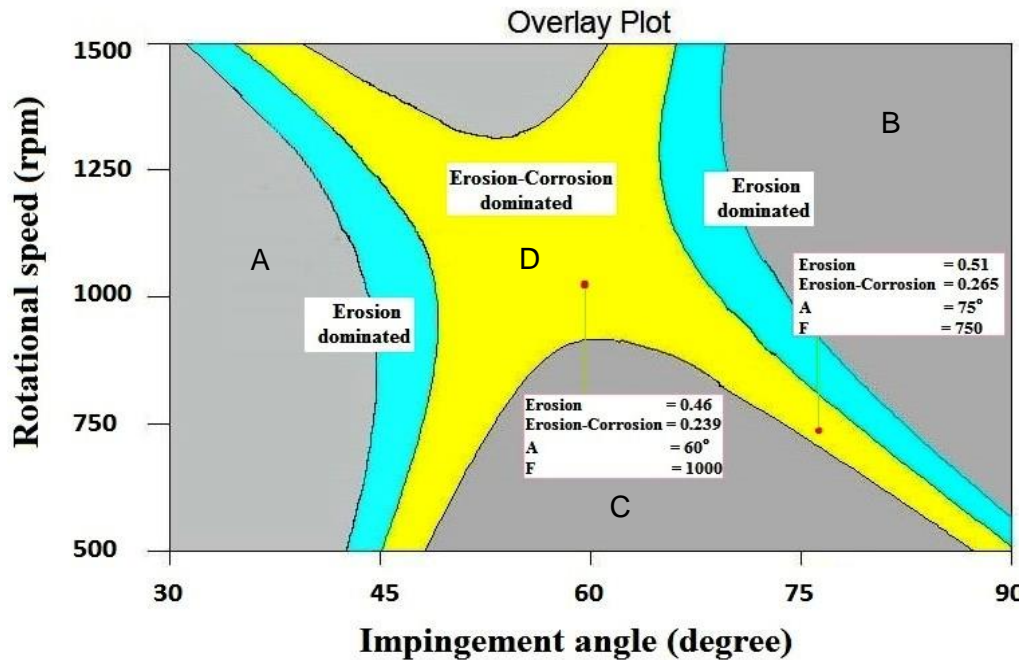


Fig. 15 Process map for erosion-corrosion synergy

Figure 15 shows the graphical representation of the material degradation mechanism such as erosion, corrosion and EC. The synergetic effect of erosion and corrosion in an important criteria for the component development for marine applications. The distinct characteristics exhibit by the ductile metal and brittle ceramic material are well proved by many researchers. There is wealth of research exists pertaining to the erosion and corrosion behavior of metals and ceramics. From the previous study, metal and ceramic shows different fashion for their material degradation. Evaluation of the erosion component and corrosion component for materials will not give better insight for applications of real time environment. Experimental condition involving assessment of the performance characteristics for erosion and corrosion shows different strategies and responses. Hence, selection of material is the important requirement for the today's scenario. In this study, an effort has been made to develop the process map for the application of WC-10Co coatings for erosion, corrosion and erosion - corrosion or synergetic effect [16].

Figure 15 shows the process map for the erosion, corrosion and erosion-corrosion synergy.

Experiments were conducted for erosion in liquid free environment, solid free environment and liquid-solid environment. To understand the behavior of 35CrMo steel and WC-10Co coatings, experiments were conducted for these materials in the above mentioned conditions.

The aim for the development of process map for Erosion, Corrosion and Erosion- corrosion shall apply for the industry use only. The developing process map for E-C synergy is only applicable for the WC-10Co coating system under the environment, experimental parameters, coating processing method and coating microstructure.

From this process map, one can find the WC-10Co coating erosion, corrosion, and erosion-corrosion performance for the given parameters. Similar kind of process maps were developed for WC-10Co coatings, only representative map is presented here. Considering the WC-10Co coating system had a porosity of 1.8 vol % sprayed by HVOF spray system. Experimental conditions are given in Table 2. Process map for erosion-corrosion, erosion and corrosion is divided into four distinct regions, such as

A – Shallow angle impingement and low – high rotational speed

B – Higher angle impingement – High rotational speed

C – Modust angle – modust speed

D – Modust angle – high rotation speed

From the progress map one can estimate the materials performance in terms corrosion dominated region according to require operational process parameter. Shallow angle impingement and low – high rotational speed area expiates erosion dominated region for ductile materials. Higher angle impingement – High rotational speed for ceramics, shows brittle nature in erosion dominated region. Modust angle – modust speed describes erosion – corrosion dominated region for materials considered for liquid solid environment. Process map can be used predate the mass loss in the fermented condition without constructing the experiment, for the consider parameter.

5. Sensitivity Analysis

Table 3 Factors considered for erosion – corrosion test and their levels

Parameters	Units	notation	Levels				
			-2	-1	0	1	2
Angle of Impingement	degrees	A	30	45	60	75	90
Rotational Speed	rpm	S	500	750	100 0	125 0	150 0
Slurry Composition	g/cc	F	200	300	400	500	600

5.1 Predictive Statistical Model for Erosion Rate

In this study, a response surface model-building technique was utilized to predict erosion-corrosion rate in terms of impingement angle, slurry composition and rotational speed. To correlate the experimental parameters and the mass loss, a second order quadratic empirical relationship was developed to predict the responses based on experimentally measured values. The responses are function of impingement angle (A), Rotational speed (S), and slurry composition (F) and it can be expressed as

$$\text{Responses} = f(A, F \text{ and } S). \quad (1)$$

The final empirical relationships to estimate the responses are given below,

$$\begin{aligned} \text{Erosion-corrosion mass loss for uncoated 35CrMo steel} = & 0.30 - 0.034 *A + 0.015 *S \\ & - 0.014 *F - 0.014 *A^2 - 5.981 \times 10^{-3} *S^2 + 0.053 *F^2 + 0.035 *A * F - 0.040 *A *S - 0.040 \\ & *F *S. \end{aligned} \quad (2)$$

$$\begin{aligned} \text{Erosion-corrosion mass loss for coated 35CrMo steel} = & 0.47 - 0.022 *A - 7.500 \times 10^{-3} \\ & *S - 0.13 *F - 8.110 \times 10^{-3} *A^2 - 0.037 *S^2 + 0.12 *F^2 + 0.027 *A *F - 0.052 *A *S \\ & - 0.045 *F *S. \end{aligned} \quad (3)$$

Table 4 Experimental design and results matrix for erosion-corrosion test

Exp. conditions	Angle of impingement (A)	Slurry composition (F)	Rotational speed (S)	Mass loss of Uncoated steel (g)	Mass loss of coated 35CrMo steel (g)
1	45	300	750	0.64	0.32
2	75	300	750	0.64	0.26
3	45	500	750	0.41	0.3
4	75	500	750	0.52	0.39
5	45	300	1250	0.82	0.51
6	75	300	1250	0.61	0.30
7	45	500	1250	0.41	0.34
8	75	500	1250	0.31	0.26
9	30	400	1000	0.48	0.32
10	90	400	1000	0.39	0.18
11	60	200	1000	1.22	0.55
12	60	600	1000	0.69	0.49
13	60	400	500	0.34	0.25
14	60	400	1500	0.31	0.31
15	60	400	1000	0.46	0.3
16	60	400	1000	0.46	0.3
17	60	400	1000	0.46	0.3
18	60	400	1000	0.49	0.32
19	60	400	1000	0.46	0.3
20	60	400	1000	0.47	0.31

Table 5 ANOVA results for uncoated 35CrMo steel substrate

Source	Sum of Squares	df	Mean square	F Value	Prob > F	
Model	0.153054	9	0.017006	470.6427	< 0.0001	Significant
A	0.018225	1	0.018225	504.3789	< 0.0001	
S	0.003412	1	0.003412	94.41702	< 0.0001	
F	0.003025	1	0.003025	83.71722	< 0.0001	
A ²	0.005166	1	0.005166	142.9616	< 0.0001	
S ²	0.0009	1	0.0009	24.8949	< 0.0005	
F ²	0.07107	1	0.07107	1966.877	< 0.0001	
AF	0.0098	1	0.0098	271.2161	< 0.0001	
AS	0.0128	1	0.0128	354.2415	< 0.0001	
FS	0.0128	1	0.0128	354.2415	< 0.0001	
Residual	0.000361	10	3.61x 10 ⁻⁵			
Lack of Fit	1.13 x 10 ⁻⁵	5	2.27 x 10 ⁻⁶	0.032387	0.9991	not significant
Pure Error	0.00035	5	0.00007			
Cor Total	0.153415	19				

Table 6 ANOVA results for coated 35CrMo steel substrate

Source	Sum of Squares	df	Mean square	F value	Prob > F	
Model	0.821538	9	0.091282	1427.196	< 0.0001	significant
F	0.275625	1	0.275625	4309.404	< 0.0001	
A	0.0081	1	0.0081	126.6437	< 0.0001	
S	0.0009	1	0.0009	14.07152	< 0.0038	
A ²	0.001653	1	0.001653	25.85246	< 0.0005	
S ²	0.03416	1	0.03416	534.0873	< 0.0001	
F ²	0.373555	1	0.373555	5840.539	< 0.0001	
AF	0.00605	1	0.00605	94.59191	< 0.0001	
AS	0.02205	1	0.02205	344.7523	< 0.0001	
FS	0.0162	1	0.0162	253.2874	< 0.0001	
Residual	0.00064	10	6.4 x 10 ⁻⁵			
Lack of Fit	9.77x10 ⁻⁶	5	1.95 x 10 ⁻⁶	0.01551	0.9998	not significant
Pure Error	0.00063	5	0.000126			
Cor Total	0.822177	19				

5.2 Checking the adequacy of the formulated empirical relationships

In this investigation, analysis of variance (ANOVA) technique was used to check the adequacy of the developed empirical relationships. ANOVA test results of the erosion-corrosion rate of uncoated 35CrMo steel and coated 35CrMo steel are presented in Tables 5 and 6. From the tables, it was found that the predominant factors (F value assessment) which have direct influence on the responses as per hierarchy are rotational speed, angle of impingement, and slurry composition respectively. Collectively, these results indicate the excellent capability of the regression model. The developed empirical relationships can be effectively used to predict the responses by substituting the experimental parameter values in coded form as desired.

Sensitivity analysis is an important tool to quantify the influence of experimental parameters on the erosion-corrosion rate. This type of analysis can also be used to control the experimental parameters during erosion-corrosion as if they are more sensitive on E-C rate. Mathematically, sensitivity of an objective function with respect to a design variable is the partial derivative of that function with respect to its variables. The sensitivity equations 4, 5, 6 represent the sensitivity on EC for impingement angle, slurry composition and rotational speed respectively.

Impact angle (A), Rotational speed (S) and slurry composition (F)

$$\partial(\text{E-C})/\partial A = -0.022 + 0.027 \times F - 7.50 \times 10^{-3} \times S + 2 - 0.811 \times A \quad \text{-----} \quad 4$$

$$\partial(\text{E-C})/\partial F = -0.13 + -0.052 \times A + 0.045 \times S + 2 \times 0.12 \times F \quad \text{-----} \quad 5$$

$$\partial(\text{E-C})/\partial S = 0.75 \times 10^{-3} + 0.052 \times A - 0.045 \times F + 2 \times 0.037 \times S \quad \text{-----} \quad 6$$

Sensitivity is analyzed here using the partial derivatives of Equations 4 through 6. Namely, positive sensitivity values imply an increment in the objective function by a small change in design parameter, whereas negative values state the opposite. To evaluate sensitivities, each input parameter should be varied while keeping all other input parameters constant to see how the responses react to these variations. An output parameter would be considered very sensitive with respect to a certain input parameter if a large change of the output parameter value is observed. Sensitivities of process parameters on E–C are presented in Table 7.

Table 7 Sensitivity analysis of erosion-corrosion rate

Angle of impingement (A)	Slurry composition (F)	Rotational speed (S)	$\partial(\text{E-C})/\partial \text{A}$	$\partial(\text{E-C})/\partial \text{F}$	$\partial(\text{E-C})/\partial \text{S}$
30	1000	400	-0.49	-1.32	0.01
45	1000	400	-0.29	-0.32	0.35
60	1000	400	-0.19	0.18	0.52
75	1000	400	-0.09	0.68	0.69
90	1000	400	-1.33	-0.52	0.55
60	500	400	-0.81	-0.42	0.45
60	750	400	-0.29	-0.32	0.35
60	1000	400	0.23	-0.22	0.25
60	1250	400	0.75	-0.12	0.15
60	1500	400	-0.03	-0.694	0.09
60	1000	200	-0.16	-0.507	0.22
60	1000	300	-0.29	-0.32	0.35
60	1000	400	-0.29	-0.32	0.35
60	1000	500	-0.04	-0.45	0.75
60	1000	600	0.21	-0.58	1.15

From Fig. 16, it can be seen that the variation of rotational speed causes large changes of E-C and also higher than that of other parameters. Considering the changes of erosion-corrosion rate, the sensitivity of E-C process parameters can be ranked as follows: rotational speed is more sensitive followed by impingement angle and slurry composition respectively. The degree to which the HVOF coating offers an enhanced performance.

Table 8 Improvement in percentage (IP %) HVOF WC-10Co coating over 35CrMo steel

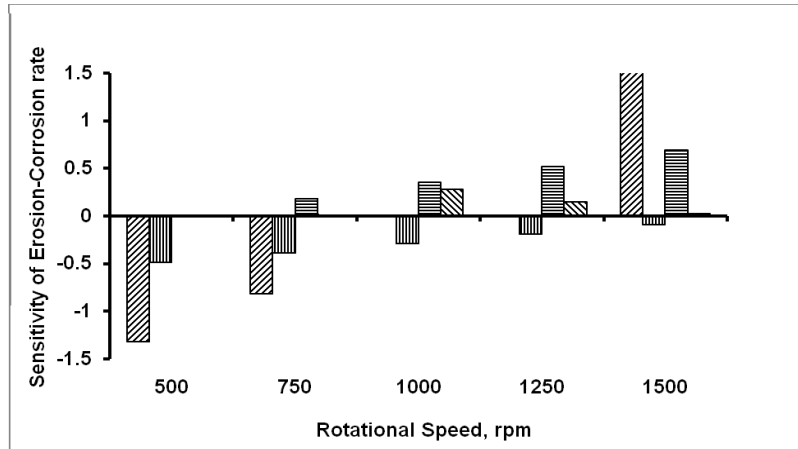
Material	Sand Load			Angle of impingement		
	500 rpm	1000 rpm	1500 rpm	30°C	60°C	90°C
35CrMo steel	80	84	80	78	65	49

Table 9 Comparison of material degradation components of 35CrMo steel with HVOF WC-10Co coating at 1000 g/cc

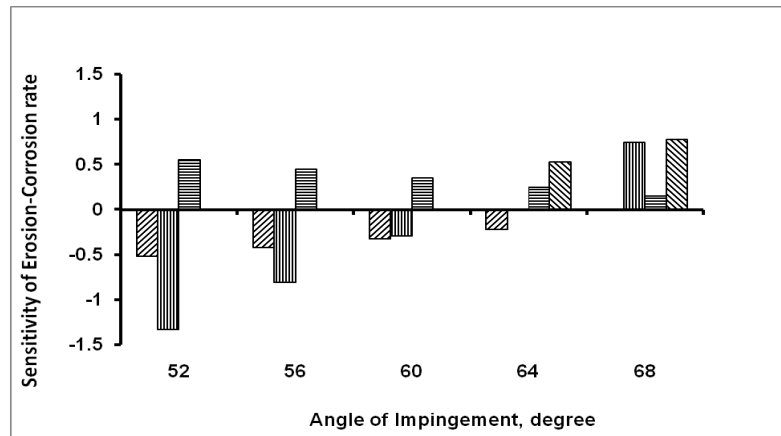
Material	Erosion (%)	Corrosion (%)	Erosion-Corrosion (%)	Hardness (Hv)
HVOF WC-Co-Cr	82	5	21	1569
35CrMo steel	91	12	42	470

Table 8 shows the improvement in E-C for the uncoated and WC-10Co coated 35CrMo steel system for the marine applications. From this study, sand rotational speed and angle of impingement are the important factors for the marine component derivative and shows 80 % improvement in sand loading and 65 % improvement were achieved in angle of impingement.

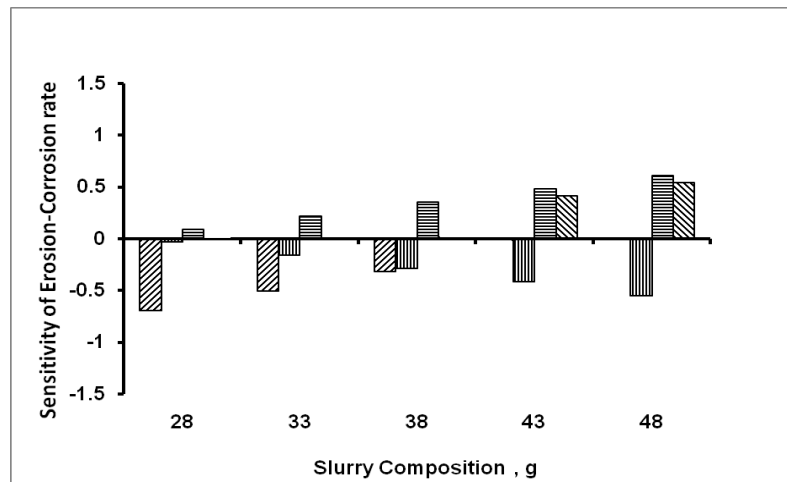
Table 9 reports the uncoated material degradation in erosion, corrosion and erosion-corrosion environment. Around four fold improvement in hardness for WC-10Co coating when compared with 35CrMo steel 11 % erosion 8 % improvement in corrosion, 25 % improvement in erosion corrosion in material degradation.



(a) Sensitivity of coated erosion – corrosion rate for rotational speed



(b) Sensitivity of coated erosion – corrosion rate for Angle of impingement



(c) Sensitivity of coated erosion – corrosion rate for slurry composition

Fig.16 Sensitivity Graphs

Conclusions

1. The damage mechanism under a liquid-solid impinging jet is very complex. However the process, is thought to be one where corrosion dissolves the matrix, erosion mechanisms involve the solid particles drilling into the coating and synergy is due to the solid particles removing the hard phase particles which are undermined by corrosive effects.
2. Process maps developed for low angle impingement – rotational speed, high angle – rotational speed, modust angle – modust speed. From this region one can determine the performance of the coatings for various environmental landing.
3. About 80 % resistance improvement in 35CrMo steel for the different solid loading conditions and 70 % improvement for angle impingement. Around four fold increased hardness value was observed in WC-10Co coating against 35CrMo steel. Hardness of 841 degradation against degradation in erosion around against 13 % in corrosion and 24.8 % against 43.2 % improvements here observed.
4. HVOF sprayed WC-10Co coatings provided the superior erosion corrosion performance than the uncoated 35CrMo steel. The erosion-corrosion studies show that the high slurry rotational speed and composition promotes the synergetic action of erosion and corrosion.

Acknowledgements

The corresponding author wishes to express his sincere thanks to the Annamalai University for extending facilities to characterize the coatings. The authors also wish to thank Mr. R. Selvendiran, Technical Assistant, CEMAJOR, Annamalai University for his help in carrying out this investigation.

REFERENCES

1. E.Poursaeidi, A. Mohammadi, N. Mohsen, L. Kaveh, *Experimental studies of erosion and corrosion interaction in an axial compressor first stage rotating blade material*, *Appl. Phys. A Mater. Sci. Process*, Vol. 124, pp. 1–15, (2018).
2. N. Gladys, V. Laura, *Laboratory and field corrosion behavior of coatings for turbine blades*, *Surf. Coatings Technol.*, Vol. 94–95, pp. 161–167, (1997).
3. W. Zhu, J.W. Wang, L. Yang, Y.C. Zhou, Y.G. Wei, R.T. Wu, *Modeling and simulation of the temperature and stress fi elds in a 3D turbine blade coated with thermal barrier coatings*, *Surf. Coatings Technol.*, Vol. 315, pp. 443–453, (2017).

4. L. Ahuja, D. Mudgal, S. Singh, S. Prakash, *A comparative study to evaluate the corrosion performance of Zr incorporated Cr₃C₂-(NiCr) coating at 900°C*, *Ceram. Int.*, Vol. 44, pp. 6479–6492 (2018).
5. G. Sun, Y. Zhang, C. Liu, K. Luo, X. Tao, P. Li, *Microstructure and wear resistance enhancement of cast steel rolls by laser surface alloying NiCr-Cr₃C₂*, *Mater. Des.*, Vol. 31, pp. 2737–2744, (2010).
6. C. Lyphout, K. Sato, S. Houdkova, E. Smazalova, L. Lusvarghi, G. Bolelli, P. Sassatelli, *Tribological properties of hard metal coatings sprayed by high velocity air fuel process*, *J. Therm. Spray Technol.*, Vol. 25, pp. 331–345, (2016).
7. X. Yang, J. Zhang, G. Li, *Cavitation erosion behaviour and mechanism of HVOF-sprayed NiCrBSi-(Cr₃C₂-NiCr) composite coatings*, *Surf. Eng.*, Vol. 34, pp. 211–219, (2018).
8. V. Matikainen, G. Bolelli, H. Koivuluoto, M. Honkanen, M. Vippola, L. Lusvarghi, P. Vuoristo, *A study of Cr₃C₂- based HVOF- and HVAF-sprayed coatings: microstructure and carbide retention*, *J. Therm. Spray Technol.*, Vol. 26, pp.1239–1256, (2017).
9. L.M. Berger, *Application of hardmetals as thermal spray coatings*, *Int. J. Refract. Met. Hard Mater.*, Vol.49, pp. 350–364, (2015).
10. T. Sahraoui, N.E. Fenineche, G. Montavon, C. Coddet, *Structure and wear behaviour of HVOF sprayed Cr₃C₂-NiCr and WC-Co coatings*, *Mater. Des.*, vol. 24, pp. 309–313, (2003).
11. V. Matikainen, S. Rubio Peregrina, N. Ojala, H. Koivuluoto, J. Schubert, Houdková, P. Vuoristo, *Erosion wear performance of WC-10Co4Cr and Cr₃C₂-25NiCr coatings sprayed with high-velocity thermal spray processes*, *Surf. Coatings Technol.*, Vol.370, pp.196–212, (2019)
12. M. Akhtari Zavareh, A.A.D.M. Sarhan, B.B. Razak, W.J. Basirun, *The tribological and electrochemical behavior of HVOF-sprayed Cr₃C₂-NiCr ceramic coating on carbon steel*, *Ceram. Int.*, Vol. 41, pp. 5387–5396, (2015).
13. ASTM B276-05. *Standard test method for apparent porosity in cemented carbides*, annual book of ASTM standards, ASTM international, (2010).

14. *ASTM C633 – 01. Standard test method for adhesion or cohesion strength of thermal spray coatings, annual book of ASTM standards, ASTM international, (2008).*
15. *Jianhua zhao, Aibin ma, Xiulinji, Jinghua jiang and Yayun bao. Slurry erosion behavior of Al_xCoCrFeNiTi_{0.5} high entropy alloy coatings fabricated by laser cladding. Metals, Vol. 8, pp. 1-12, (2018)*
16. *H. Ding, Z. Dai, S.C. Skuiry, D. Hui, Corrosion wear behaviors of micro-arc oxidation coating of Al₂O₃ on 2024Al in different aqueous environments at fretting contact, Tribology Int., Vol. 43, pp. 868–875, (2010).*